Influence of Contraction Section Shape and Inlet Flow Direction on Supersonic Nozzle Flow and Performance

LLOYD H. BACK*, ROBERT F. CUFFEL†, AND PAUL F. MASSIER‡
Jet Propulsion Laboratory, Pasadena, Calif.

Wall static pressure measurements and performance parameters are presented for axisymmetric supersonic nozzles with relatively steep convergent sections and comparatively small radius-of-curvature throats. The nozzle walls were essentially adiabatic. These results are compared with those obtained in other nozzles tested previously to appraise the influence of contraction shape on performance. Both the flow coefficient and the thrust were less than the corresponding values for one-dimensional, isentropic, plane flow for both the axial and radial inflow nozzles considered, but the specific impulse, the most important performance parameter, was found to be relatively unchanged. The thrust decrement for the axial inflow nozzles was established primarily by the shape of the contraction section, and could be estimated reasonably well from a conical sink flow consideration. The radial inflow nozzle has a potential advantage from a cooling point of view if used in a rocket engine.

Nomenclature

A = plane cross-sectional area
A_s = surface area of spherical cap
C_D = mass flow coefficient
ΔC_F = thrust decrement, Eq. (3)
c_c = specific heat at constant pressure
D = diameter
f = function, Eq. (4)
F = axial force
I = specific impulse
$\dot{m}$ = mass flow rate
M = Mach number
p = pressure
Q = total heat transfer from nozzle inlet to throat
r = radius
r_c = throat radius of curvature
r_{th} = throat radius
R = spherical radial distance or gas constant
$Re_{D_{th}}$ = throat Reynolds number, $(\rho_e u_e D/\mu_e)_{th}$
T = temperature
$\bar{T}_w$ = average wall temperature from nozzle inlet to throat
u = axial velocity
u_r = radial velocity
V = spherical radial velocity
$\tilde{V}$ = either V or u
z = axial distance
γ = specific heat ratio
ε_c = nozzle contraction area ratio
ε_e = nozzle expansion area ratio
λ = divergent half-angle
μ = viscosity
ρ = density
σ = convergent half-angle

Subscripts and Superscripts

a = ambient condition
c = conical sink flow condition
e = nozzle exit condition or local freestream condition
i = nozzle inlet condition
t = stagnation condition
tan = circular arc—conical tangency upstream of throat
th = throat condition
w = wall condition
1-D = one-dimensional, isentropic, plane flow condition
$(\bar{\ })$ = average value across flow

Introduction

THIS investigation is concerned with the influence of the shape of the contraction section and the direction of the entering flow on the flowfield and performance of axisymmetric, supersonic nozzles. Air entered the nozzles either in the axial or radial direction. The axial-inflow nozzles have conical convergent sections and circular arc throat sections. A channel, perpendicular to the axis, formed the inlet of the radial-inflow nozzle. Wall static pressure measurements along the nozzles and internal flow measurements at the nozzle inlets provided the basis for evaluating the contribution of the various sections of the nozzles to the thrust, as well as establishing the over all thrust by application of a momentum balance on the flow. The flow coefficient and specific impulse are also presented for the nozzles.

The investigation was motivated by an interest in nozzles which have a relatively steep convergent section and a comparatively small radius of curvature at the throat. Such nozzles are shorter, weigh less, and have a smaller surface area (and, hence, a lower total heat load in rocket engine applications) than conventional nozzles used in propulsion devices.

Nozzle Descriptions and Measurements

Measurements are reported for an axial inflow nozzle which has a 75° half-angle convergent section and a ratio of throat radius of curvature to throat radius r_c/r_{th} of 0.25. The performance of this nozzle is appraised relative to other axial inflow nozzles that have been previously tested at JPL.[1-3] The half-angle σ of the conical convergent sections of the axial inflow nozzles (Table 1) ranged from 30° to 75° and the ratio r_c/r_{th} ranged from 0.25 to 2.0. The contraction area ratio ε_c was on the order of either 10 or 100. Some of the inlet sections consisted of circular arcs of radius r_{c_i} and for others the inlet tube and convergent cone were joined without smoothing the corner, i.e., $r_{c_i} \to 0$. All of the nozzles had conical divergent sections with the same value of the half-angle λ of 15°. The expansion area ratio ε_e ranged from 2.3 to 9. Some of the nozzle walls were essentially adiabatic and some were externally cooled. Viscous (boundary layer) effects on performance should not have been significant for the relatively high Reynolds number flows considered (throat

Received April 30, 1971; revision received January 18, 1972. This work presents the results of one phase of research carried out in the Propulsion Research and Advanced Concepts Section of the Jet Propulsion Laboratory, California Institute of Technology, under Contract NAS 7-100, sponsored by NASA.
Index category: Nozzle and Channel Flow.
* Member Technical Staff. Associate Fellow AIAA.
† Member Technical Staff. Member AIAA.
‡ Group supervisor. Associate Fellow AIAA.

Table 1 Experimental data for axial-inflow nozzles; all nozzles, $\lambda = 15°$

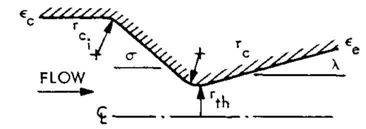

SOURCE	REF	σ, deg	$\frac{r_c}{r_{th}}$	r_{th}, in.	r_{c_i}, in.	ϵ_c	ϵ_e	$Re_{D_{th}}$	T_w	C_D	$\left(\frac{F}{F_{1-D}}\right)_e$ MEASURED	$\left(\frac{F}{F_{1-D}}\right)_e$ EQ. (11)	$\left(\frac{I}{I_{1-D}}\right)_e$
PRESENT RESULTS	---	75	0.25	0.800	1.00	9.76	2.3	1.0×10^6 TO 3.5×10^6	$\sim T_{aw}$	0.951	0.941	0.932	0.989
BACK, MASSIER AND GIER	1	45	0.625	0.800	0.80	9.76	6.60	1.8×10^6	$\frac{T_w}{T_{to}} = 0.45$	0.983	0.971	0.972	0.988
								TO	TO				
		30	2.0	0.902	1.42	7.90	2.66	3.0×10^6	0.58	0.990	0.981	0.975	0.991
NORTON AND SHELTON	2,3	30	0.35	0.563	0	102	9.0	5.9×10^6	$\sim T_{aw}$	0.970	0.976	0.983	1.006
			0.55							0.969	0.976	0.984	1.007
			0.75							0.982	0.979	0.985	0.997
		30	1.0	0.563	0	102	9.0	5.9×10^6	$\sim T_{aw}$	0.983	0.991	0.986	1.008

Reynolds numbers $Re_{D_{th}}$ above one million) and the relatively small expansion area ratios of the nozzles.

The radial inflow nozzle for which measurements are reported consisted of a plane inlet section perpendicular to the axis, a circular arc convergent section between the inlet and the throat, and a specially contoured section that connected the throat to the conical divergent section. The ratio of the throat radius of curvature to throat radius r_c/r_{th} was 0.49; the throat radius was 0.800 in.; the radius of the contoured section had a continuous second derivative with respect to the axial distance; the divergent half-angle was 15°, and the expansion area ratio was 2.3. The endwall was a circular disk parallel to and spaced 1.0 in. from the plane inlet wall of the nozzle.

The present steady flow tests were conducted in the auxiliary flow channel of the JPL hypersonic wind tunnel.[4] Air flowed through a venturi meter, a plenum chamber, a contraction section, a duct, and then through the nozzle from which it exhausted into an evacuated chamber. A 5.0-in. constant diameter duct 8.8 in. long preceded the 75° axial inflow nozzle. Air flowed around the outer periphery of the circular endwall placed in a larger 17-in. diameter duct upstream to enter the other nozzle radially inward. Wall static pressure taps, 0.005 in. diameter, were located at close intervals along the nozzles (and endwall). These taps, the locations of which spiraled around the nozzle walls (and endwall), were connected to mercury or oil manometer boards. The axial and the radial locations of the taps were measured within 0.001 in.

Tests were conducted over a range of stagnation pressures from 24 to 86 psia and at a stagnation temperature of about 530°R with the 75° axial inflow nozzle, and at 100 psia and 540°R with the radial inflow nozzle, as determined from pitot tube and thermocouple probe measurements upstream of the nozzles. Since the stagnation temperatures were essentially the ambient temperature, the nozzle walls (and endwall) were nearly at the adiabatic wall temperature. At a stagnation pressure of 86 psia the boundary layer in the duct one inch upstream of the inlet of the 75° axial inflow nozzle was turbulent and extended to about 10% of the duct radius. The inlet velocity distribution for the radial inflow nozzle is described subsequently. The boundary-layer measurements were made with a 0.005-in. high, flattened pitot tube.

The results obtained with the axial-inflow nozzles are discussed first and then the results are presented for the radial-inflow nozzle.

Axial Inflow Nozzles—Results

Wall Static Pressure Measurements and Flowfield

The wall contour of the 75° nozzle and the measured wall static pressures normalized by the stagnation pressure are shown in Fig. 1. The data shown represent average values of tests at stagnation pressures of 75 psia and 86 psia, and are essentially the same on a normalized basis as those obtained at a lower stagnation pressure of 25 psia. Similar distributions of the normalized pressure are expected if viscous effects were negligible. The one-dimensional, isentropic, plane flow prediction ($\gamma = 1.4$) is shown as a reference curve to indicate the large deviations that are observed because of the nozzle configuration. It is evident that the small value of r_c/r_{th} of 0.25 for this nozzle had a significant influence on the wall pressure distribution and therefore the flowfield in the throat region. For example, see Ref. 5 for internal flow measurements in the 45° nozzle which has a larger value of r_c/r_{th} of 0.625. At the physical throat the Mach number near the wall is as large as 1.7. The pressure rise downstream of the tangency between the circular arc throat and the divergent conical section is associated with a compressive turning of the flow and the subsequent formation of a relatively weak shock wave as has been observed in the 45° nozzle.[6] A better view of the pressure distribution in the constant diameter duct and in the inlet of the nozzle is seen in the enlarged scale of Fig. 2. In this region the flow is compressed in turning to follow along the wall. The measured pressure rise was probably sufficient to separate the boundary layer similar to that observed in the 45° nozzle[7] which had a more gradual contraction section. Inference from the measured pressure distribution and the measurements in Ref. 7 indicates that the flow reattached along the latter portion of the curved inlet section.

Both of the measured pressure rises (adverse pressure gradients) in the nozzle inlet region and downstream of the throat play an important role in the development of the shear layer and the thermal resistance across the thermal boundary

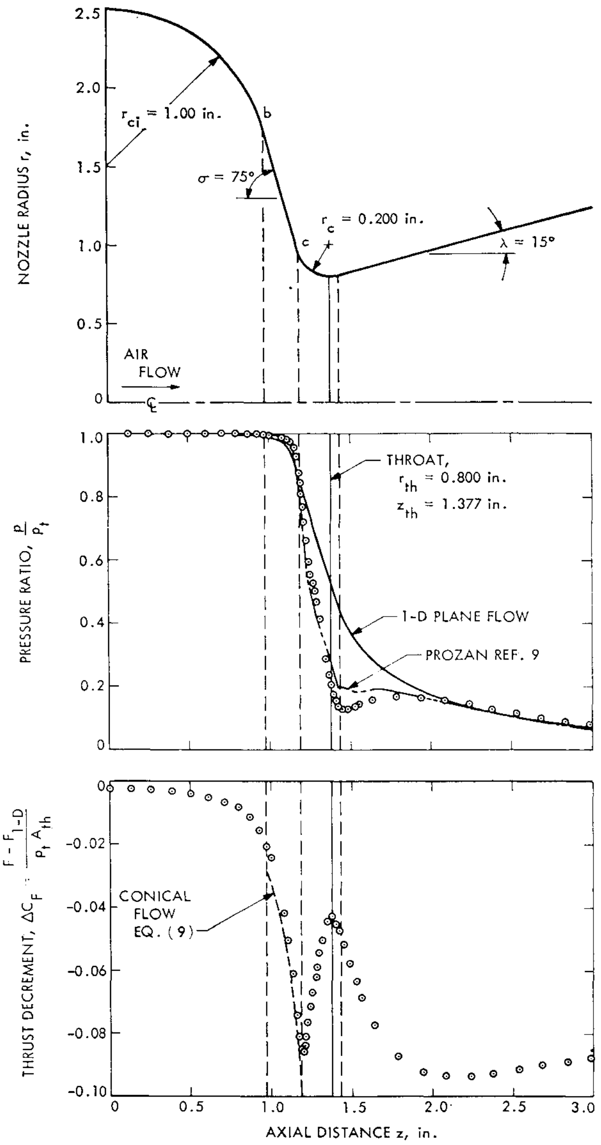

Fig. 1 Pressure distribution and thrust decrement for the 75° axial-inflow nozzle.

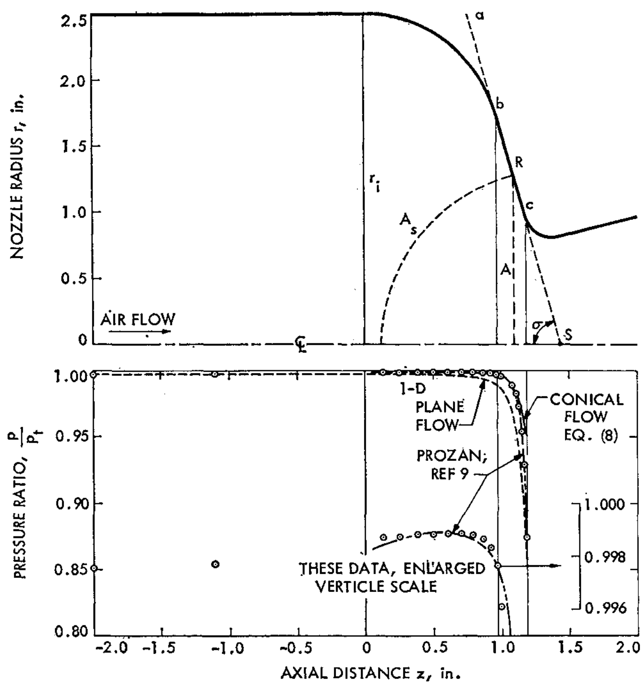

Fig. 2 Pressure distribution in the convergent section of the 75° axial-inflow nozzle and conical flow model.

layer in applications involving wall cooling.[7,8] The present results do not provide any information in this regard, however because the nozzle was not instrumented to obtain heat-transfer data.

A prediction by Prozan[9] of the pressure distribution along the wall is shown in Figs. 1 and 2. These calculations involve the numerical solution of the continuity and irrotational equations for steady flow by using an error minimization relaxation technique.[10] The predicted pressure distribution is in fairly good agreement with the measurements. A pressure rise is predicted in the inlet region and downstream of the throat, but the magnitude is less than observed experimentally downstream of the throat.

Flow Coefficient

The flow coefficient C_D, defined in the usual way as the ratio of the actual mass flow rate to the computed value for one-dimensional, plane, isentropic flow, was 0.951 ± 0.005. The actual mass flow rate was determined by use of a venturi. Flow coefficients for the 75° nozzle, for the other nozzles in Table 1, and for nozzles tested by other investigators are discussed in Ref. 11.

Thrust

The thrust was obtained by application of a momentum balance on the flow and by using the thrust expression if the nozzle were used in a rocket, i.e.,

$$F_e = \dot{m}\bar{u}_e + (\bar{p}_e - p_a)A_e \tag{1}$$

For the situation where the ambient pressure is zero (vacuum) and the shear force is negligible compared to the pressure force on the nozzle side wall, the thrust is

$$F_e = \dot{m}\bar{u}_i + \bar{p}_i A_i + \int_{Ai}^{Ae} p\, dA \tag{2}$$

The actual thrust is then normalized with respect to that for a one-dimensional plane isentropic flow $(F/F_{1-D})_e$, i.e., by applying Eq. (2).

Before discussing these thrust ratios, it is informative to examine the relative contribution to the thrust of the various sections of the nozzle. This was done by applying Eq. (2) locally along the nozzle, not only at the exit, and comparing the result to that for a one-dimensional, plane, isentropic flow in terms of a thrust decrement defined as

$$\Delta C_F = (F - F_{1-D})/p_t A_{th} \tag{3}$$

In Eq. (3) $F = \dot{m}\bar{u}_i + \bar{p}_i A_i + \int_{A_i}^{A} p\, d\, A$. The thrust decrement is shown in the lower part of Fig. 1. The magnitude of the thrust decrement increases, i.e., larger negative values, along the curved section and the conical convergent section. This occurs because measured pressures are higher than those for one-dimensional, plane, isentropic flow in this region. Therefore, the larger axial force on the side wall subtracts from the thrust which acts in the -z direction if the nozzle were used in a rocket. A local minimum in the thrust decrement occurs near the end of the conical convergent section where the measured pressures become less than the one-dimensional flow values. Through the throat section where the measured pressures lie below the one-dimensional flow values, the thrust decrement first increases and then decreases again because the orientation of the axial forces on the nozzle side wall changes direction in passing through the throat. Downstream of the throat the

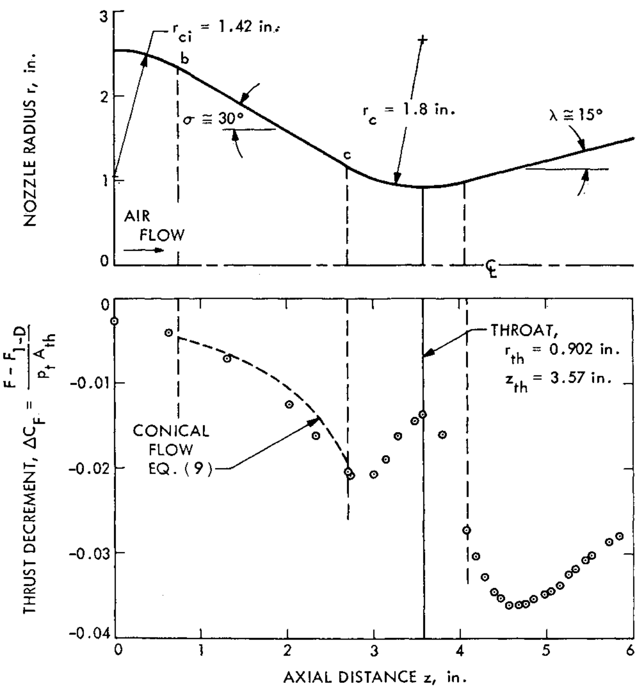

Fig. 3 Thrust decrement for the 45° axial-inflow nozzle of Ref. 1.

thrust decrement continues to decrease until the measured pressures exceed the one-dimensional flow values. The thrust decrement then begins to rise again slightly.

Similar distributions of the thrust decrement are shown in Figs. 3 and 4 for nozzles tested in previous investigations, but for which the thrust decrement was not shown. They differ in magnitude because of the different nozzle configurations.

An interesting observation for these comparatively low expansion area-ratio nozzles is that the thrust decrement for each nozzle is essentially that value at the end of the conical convergent section, i.e., the net effect of the throat section and the divergent section on the thrust decrement is virtually negligible because the smaller axial force on the nozzle sidewall between the end of the conical convergent section and the throat that decreases the thrust decrement is offset by the smaller axial force downstream of the throat that increases the thrust decrement.

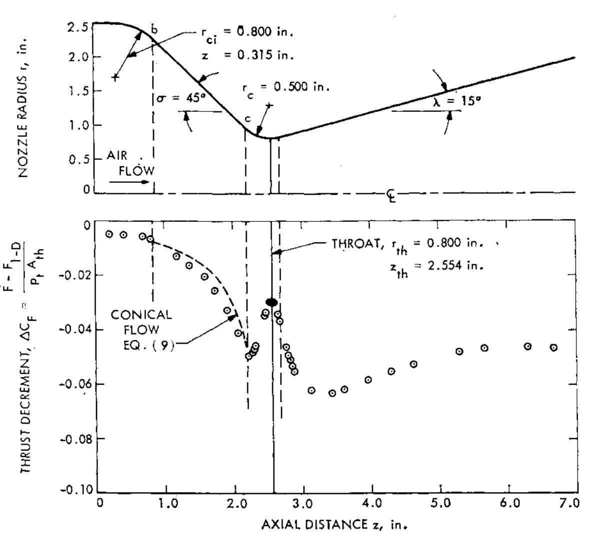

Fig. 4 Thrust decrement for the 30° axial-inflow nozzle of Ref. 1.

Conical Sink Flow Consideration

Since the thrust decrement for these nozzles is apparently determined by the shape of the contraction section up to the tangency between the conical section and the circular-arc throat, a conical sink flow prediction may be used as a first approximation to calculate the thrust for these nozzles. The conical sink flow model is developed in this section and the predictions based on this model are compared to the experimentally evaluated flow along the wall and to the experimental thrust.

A fictitious conical nozzle is shown by the dashed curve in Fig. 2 which has the same convergent half angle σ as the actual nozzle and has a sink located at s along the axis. Along any spherical cap whose surface area is A_s the radial velocity V is invariable and only depends upon the radial distance R from the sink. From geometry, the surface area of the spherical cap is related to the planar cross-sectional area A by

$$A_s = A/f \text{ where } f = \sin^2 \sigma/2(1 - \cos \sigma) = \tfrac{1}{2}(1 + \cos \sigma) \quad (4)$$

The function f varies from 1 for $\sigma = 0$ to $\frac{1}{2}$ for $\sigma = 90°$. Since the flow is essentially incompressible in the contraction region,§ the requirement that the mass flow rate for conical flow be the same as for plane flow, i.e.,

$$A_s V = Au \quad (5)$$

then establishes that the radial velocity V is always less than the average axial velocity u

$$V = fu = f\left(\frac{A_{th}}{A}\right)\left[RT_t\gamma\left(\frac{2}{\gamma+1}\right)^{\frac{\gamma+1}{\gamma-1}}\right]^{1/2} \quad (6)$$

since $f < 1$. The last relationship for u in this equality was obtained from the conservation of mass applied along the nozzle for plane flow, $A\ \rho u = \dot{m}_{1-D}$, and in the contraction region $\rho = \rho_t = p_t/RT_t$ for a perfect gas. Therefore, the momentum equation

$$dp/\rho + \tilde{V}\, d\tilde{V} = 0 \quad (7)$$

where $\tilde{V}$ is either V or u, indicates that for a given stagnation pressure the static pressure will be higher along the conical wall for conical flow than for the axial flow case as is observed experimentally. Integration of Eq. (7) along the conical flow and combination of the resulting equation with Eq. (6) give the wall static pressure distribution

$$\left(\frac{p}{p_t}\right)_c = 1 - \frac{\rho V^2}{2p_t} = 1 - \left(\frac{A_{th}}{A}\right)^2 \frac{\gamma}{2}\left(\frac{2}{\gamma+1}\right)^{\frac{\gamma+1}{\gamma-1}} f^2 \quad (8)$$

The predicted wall static pressure is shown in Fig. 2 for the 75° nozzle: $f = 0.63$ and $\gamma = 1.4$ for air flow. At the tangency point b, the predicted pressure based on conical sink flow is considerably above the predicted plane flow value and is near the measured value. Along the conical section the predicted conical flow pressures cross the measured values and by the time the flow has reached point c where the throat curvature begins, they lie above the measured pressures. It is evident that the actual flow along the conical section is not described too well by conical flow theory. If compressibility effects were included the correspondence with the measurements would be only slightly better near the end of the conical section. However, since the over all pressure level along the conical section agrees fairly well in magnitude with the measurements, the thrust decrement can still be estimated reasonably well.

§ The analysis was also carried out by including compressibility effects—the final result appears later.

For either conical or plane one-dimensional flow the general expression for the thrust for a rocket nozzle discharging into a vacuum is

$$F = (p + \rho \tilde{V}^2)A$$

By application of this relation along the convergent section as before, where the flow is essentially incompressible, the thrust decrement is

$$\Delta C_F = \frac{F_c - F_{1-D}}{p_t A_{\text{th}}} = \left(\frac{A}{A_{\text{th}}}\right)\frac{1}{2}\frac{\rho}{p_t}(V^2 - u^2)$$

This can be rewritten as follows by using Eq. (6).

$$\Delta C_F = \left(\frac{A_{\text{th}}}{A}\right)\frac{\gamma}{2}\left(\frac{2}{\gamma+1}\right)^{\frac{\gamma+1}{\gamma-1}}(f^2 - 1) \tag{9}$$

The magnitude of the thrust decrement increases as one proceeds in the flow direction along the convergent section as A decreases. Its magnitude also increases for different nozzles as the conical half angle increases because f becomes less than unity. The sign of ΔC_F is always negative, i.e., it is a decrement for inviscid flow.

Predicted values of the thrust decrement for conical sink flow based on Eq. (9) are shown in Figs. 1, 3, and 4 along the conical convergent sections of the nozzles. In general, there is relatively good agreement with the measurements.

As a first approximation, the actual thrust for conical nozzles can be estimated by evaluating ΔC_F at the tangency between the conical convergent section and the throat section, i.e., from Eq. (9).

$$\Delta C_{F_{\tan}} = \left(\frac{A_{\text{th}}}{A_{\tan}}\right)\frac{\gamma}{2}\left(\frac{2}{\gamma+1}\right)^{\frac{\gamma+1}{\gamma-1}}(f^2 - 1) \quad \text{where}$$

$$\frac{A_{\tan}}{A_{\text{th}}} = \left[1 + \frac{r_c}{r_{\text{th}}}(1 - \cos\sigma)\right]^2 \tag{10}$$

Next, the definition of ΔC_F is used to obtain the following result since $\Delta C_{F_e} \cong \Delta C_{F_{\tan}}$

$$\left(\frac{F_C}{F_{1-D}}\right)_e = 1 + \frac{\Delta C_{F_{\tan}}}{(F_{1-D}/p_t A_{\text{th}})_e} \tag{11}$$

The expression for $A_{\text{th}}/A_{\tan}$ in Eq. (10) follows from the geometry of the conical convergent section and circular arc throat.

Thrust ratios obtained from Eq. (11) with $(F_{1-D}/p_t A_{\text{th}})_e$ obtained from the usual one-dimensional, plane, isentropic flow value for a nozzle discharging into a vacuum are shown in Table 1. They compare favorably with the measured values as expected since such an estimate of the thrust is predicated on the observed correspondence of the predicted thrust decrement at the tangency location with that measured at the nozzle exit. In this regard Fig. 5 indicates the estimated influence of the ratio of the throat radius of curvature to throat radius r_c/r_{th} and the convergent half-angle σ on the thrust decrement. Clearly, nozzles with relatively small values of r_c/r_{th} and steep convergent sections, i.e., large σ, have larger thrust decrements.

By allowing for compressibility effects in the conical sink flow and the plane, one-dimensional flow, the thrust decrement at the tangency is given by

$$\Delta C_{F_{\tan}} = \left[(1 + \gamma M_c^2)\frac{p_c}{p_t} - (1 + \gamma M_{1-D}^2)\frac{p_{1-D}}{p_t}\right]_{\tan}\frac{A_{\tan}}{A_{\text{th}}} \tag{12}$$

$M_{c_{\tan}}$ and $(p_c/p_t)_{\tan}$ can be evaluated from isentropic flow tables for the effective area ratio $(A_{\tan}/f)(1/A_{\text{th}})$. The solid curves in Fig. 5 indicate the effect of compressibility on the

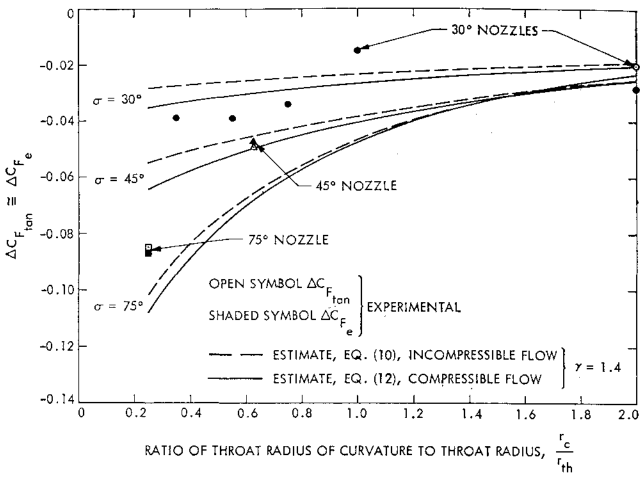

Fig. 5 Influence of the radius ratio r_c/r_{th} and convergent half angle σ on the thrust decrement for axial-inflow nozzles.

estimated thrust decrement. It appears that the relation given by Eq. (10) which explicitly indicates the influence of nozzle shape is adequate to use as a first approximation.

Specific Impulse

The most important performance indicator is the specific impulse ratio $(I/I_{1-D})_e$, which is the ratio of $(F/F_{1-D})_e$ to the flow coefficient C_D. Values of $(I/I_{1-D})_e$ shown in Table 1 are seen to differ little from unity for the nozzles considered. This occurs because the specific impulse $I_e = F_e/\dot{m}$ depends primarily on the average axial velocity component $\bar{u}_e$ at the nozzle exit, e.g., Eq. (1), and thus is rather insensitive to the detailed nature of the flow through the convergent portion of the nozzle. This certainly would be the case for nozzles with relatively large expansion area ratios, although for such nozzles viscous effects become important and the thrust ratio, and thus the specific impulse ratio, becomes relatively less.

In this connection it should be noted that the specific impulse ratio is not given simply by the divergence factor $(\frac{1}{2})(1 + \cos\lambda)$ obtained from conical source flow theory for nozzles with relatively large expansion area ratios discharging into a vacuum. For a divergent half angle λ of 15° the divergence factor is 0.983. Actual values for I/I_{1-D} along the divergent section are shown in Fig. 6. In Ref. 6 pressure

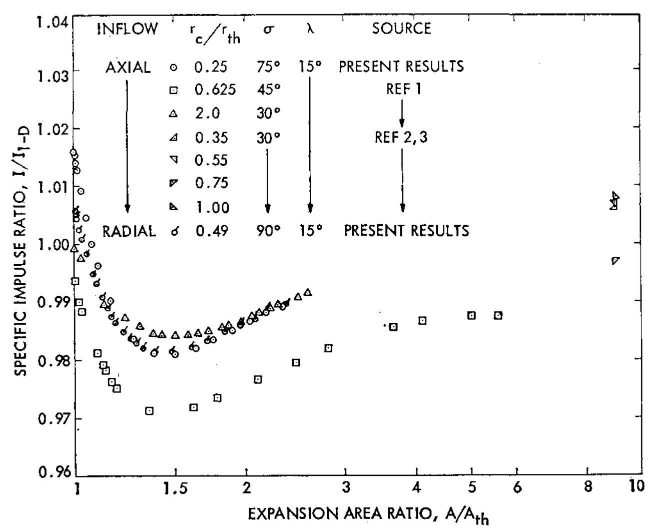

Fig. 6 Specific impulse ratio along the divergent section of the nozzles.

measurements along the centerline as well as the wall reveal the nonconical nature of the flow in the divergent section for the 45° nozzle in particular. This was also noted in Ref. 1, Fig. 1, by comparison of a conical source flow prediction to the measurements obtained with the 30° nozzle. It should be mentioned that the thrust ratios quoted in Ref. 1 which were calculated from Eq. (2) but without the entering momentum term $\dot{m}\bar{u}_i$ are essentially the same as those presented herein for the 30° and 45° nozzles because the magnitude of the entering momentum term was relatively small for those fairly large contraction area ratio nozzles.

Comments on other Investigations

Some comments should be made with regard to other measurements shown herein and also measurements obtained by other investigators. The thrust ratios shown in Table 1 for the nozzles of Norton and Shelton were obtained from thrust measurements by Thiokol[12] corrected for discharge into a vacuum. These values agree reasonably well with those obtained by Norton and Shelton[3] from their wall static pressure measurements (see Ref. 12, Figs. 3–8) although there were only a few pressure taps along the conical convergent section. The mass flow rate through these nozzles was measured with the same venturi as used in this investigation. It is not clear why some of the values of the specific impulse ratio $(I/I_{1-D})_e$ shown in Table 1 and Fig. 6 exceed unity, and this may well be associated with the accuracy of the measurements. In this regard, values of $(I/I_{1-D})_e$ shown for the 45° nozzle in Fig. 6 probably are a little low.

It is difficult to accept the absolute magnitude of the thrust measurements by Durham[13] for a large number of nozzles that were made in a blow-down facility because all of the results are given relative to a reference nozzle that had a convergent half angle of 30°, a value of r_c/r_{th} of 2, and a contoured divergent section with an expansion area ratio of 4. Durham gives the following values for the reference nozzle: $C_D = 0.985$, $(F/F_{1-D})_e = 0.95$ and consequently, $(I/I_{1-D})_e = 0.965$. The flow coefficient appears to be realistic for this reference nozzle as well as for other nozzles that he tested, e.g., see Ref. 11; but the thrust ratio appears to be too low in light of the results presented herein. For example, from Fig. 5 and Eq. (11) the estimated value of (F/F_{1-D}) is 0.988, a value closer to unity. Therefore, the specific impulse ratio $(I/I_{1-D})_e$ probably should be about unity for this reference nozzle. Consequently, the absolute magnitude of the thrust and specific impulse ratios given by Durham are in question although comparisons between the nozzles that he tested are probably valid. In this latter connection Durham mentions in Ref. 14 that there was hardly any change in the specific impulse ratios relative to that for the reference nozzle for convergent half angles larger than 30° and values of r_c/r_{th} less than 2.

Radial Inflow Nozzle Results

Radial Inflow Velocity Distribution

The axial distribution of the velocity across the radial flow channel at a location 3.0 in. from the nozzle axis is shown in Fig. 7. The Mach number in the free-stream flow at this point was about 0.06. The boundary layer was relatively thin being about 0.1 in. thick. The momentum thickness θ, the displacement thickness δ^* and the momentum thickness Reynolds number are indicated in Fig. 7. Inspection of the velocity profiles on a semilogarithmic basis indicated that the boundary layer was turbulent which is consistent with the magnitude of the values of δ^*/θ and $(\rho u_r \theta/\mu)_e$.

Viscous (boundary layer) effects should not have been significant along the nozzle wall for the relatively high Reynolds number flow considered and the relatively small

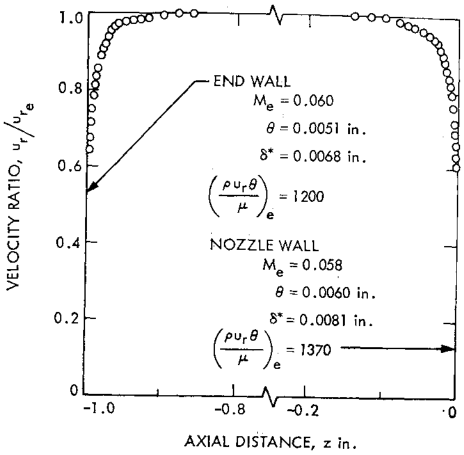

Fig. 7 Velocity distribution in the radial inflow.

expansion area ratio. However, the boundary layer on the endwall is important as will be discussed. The throat Reynolds number $Re_{D_{th}}$ was 4.2×10^6.

Wall Static Pressure Measurements and Flowfield

Wall static pressure measurements along the endwall and along that part of the nozzle wall which was parallel to the endwall are shown in Fig. 8. Mach numbers in the free-stream were obtained assuming an isentropic expansion ($\gamma = 1.4$) from the stagnation pressure to the measured wall static pressures. The radially inward flow accelerated because of the decreasing circumferential cross-sectional area. At large radial distances from the nozzle axis the pressures were virtually the same on the endwall as on the nozzle wall. At smaller radii the pressure along the endwall was slightly less than along the nozzle wall although the differences in Mach numbers are small. In the major part of this radial inflow region the Mach number distribution can be estimated closely by using the ratio of the circumferential cross-sectional area to the throat cross-sectional area as the effective area ratio for isentropic flow. This prediction is shown by a dashed curve in Fig. 8.

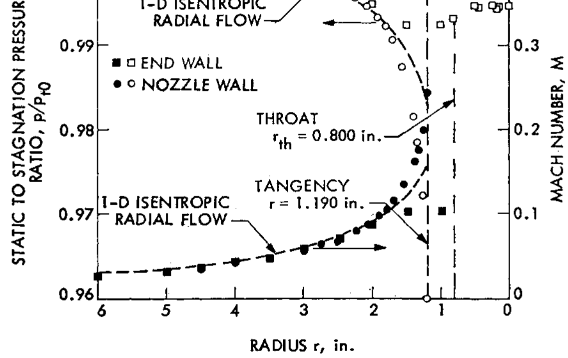

Fig. 8 Measurements along the parallel endwall and inlet wall of the radial-inflow nozzle.

As the flow near the endwall approached the radius at which the curved convergent section of the nozzle began, it reached a local maximum speed and then decelerated while experiencing an adverse pressure gradient. This adverse pressure gradient is believed to have separated the boundary layer in the vicinity of the location marked S in Fig. 8. In the center portion of the endwall the recirculating reverse flow region believed to exist there is shown diagrammatically. The pressure along the endwall decreased radially outward from its center similar to that in stagnation flow regions. Of note is that the largest freestream Mach number along the endwall was about 0.1 before the flow decelerated. However, in the freestream near the nozzle wall at the tangency the Mach number was 0.24.

Flow along the remainder of the nozzle wall, i.e., the circular arc and the divergent sections, is shown in Fig. 9. The one-dimensional, isentropic, plane flow prediction ($\gamma = 1.4$) is shown as a reference curve to indicate the large deviations that occur because of the throat configuration, as also has been observed in nozzles with axial inflow, e.g., Fig. 1 and Ref. 5. At the throat the Mach number near the wall was 1.44. The pressure rise downstream of the tangency between the contoured section and the conical divergent section is associated with an apparent overturning of the flow as it passed through the throat.[6] It exists despite the gradual contour which for this nozzle has a continuous second derivative between the circular arc throat and the conical divergent section. The flow near the wall eventually recovered from the influence of the throat configuration and agrees fairly well with the one-dimensional plane flow prediction along the divergent section. These trends are familiar and are even more exaggerated for the 75° axial inflow nozzle which had a smaller throat radius of curvature ($r_c/r_{th} = 0.25$).

Performance Parameters

The flow coefficient, defined, in the usual way, was 0.969 ± 0.005. It is less than unity primarily because of the throat configuration, similar to the axial-inflow nozzles, e.g., Ref. 11.

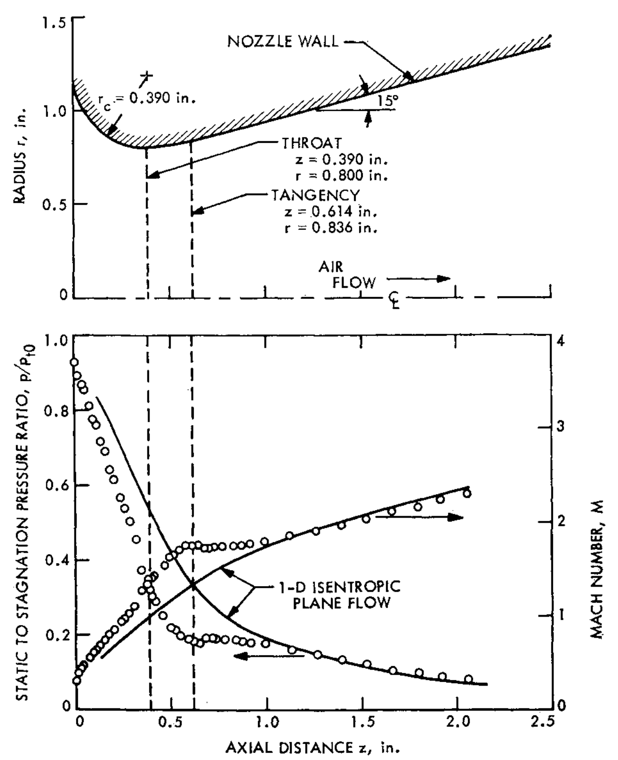

Fig. 9 Measurements along the side wall of the radial-inflow nozzle.

The analogous expression for the thrust for a radial inflow nozzle is

$$F_e = \int_0^{A_i} p dA - \int_{A_{tan}}^{A_i} p dA + \int_{A_{tan}}^{A_e} p dA$$

In this relation the first term is the force on the endwall; the second term is the force on that portion of the nozzle wall which is parallel to the endwall; and the third term is the axial force on the remainder of the nozzle wall. It is compared to the thrust that would be obtained for a nozzle discharging into a vacuum if the exit flow were one-dimensional, axial and had expanded isentropically from the same reservoir condition. The thrust ratio $(F/F_{1-D})_e$ obtained in this manner was 0.959.

Even though the mass flow rate and the thrust are less by 3% and 4%, respectively, than values associated with ideal one-dimensional plane flow, the change in specific impulse is smaller, i.e., $(I/I_{1-D})_e$ is 0.99, or 1% less than ideal. This value compares favorably with values for the axial-inflow nozzles (Table I).

The distribution of I/I_{1-D} along the divergent section of the nozzle is shown in Fig. 6. This distribution is similar in shape in the divergent section to that observed in axial inflow nozzles.

Application

The radial-inflow nozzle is believed to have advantages from a cooling point of view based upon information that has been obtained for axial-inflow nozzles. This is indicated in Fig. 10 where the total heat transfer between the inlet and the throat is shown for two axial inflow nozzles.[8,15] The throat radius and the contraction area ratio are virtually the same for the two nozzles but they have different convergent half-angles of 10° and 45°. The total heat transfer is shown in terms of a group that correlates heat-transfer data for turbulent boundary layers where

$$[Q/(T_t - \bar{T}_w)\dot{m}c_p]\alpha(\rho_i u_i/\mu_i)^{-1/5}$$

In Fig. 10 this total heat-transfer group is shown as a function of throat Reynolds number. The magnitude of the heat-transfer group is larger for the 10° nozzle primarily because it had a greater surface area than the 45° nozzle. At throat Reynolds numbers below about one million the heat-transfer group decreases for the 10° nozzle because of a reduction in turbulent transport associated with flow acceleration. This process has been referred to as partial laminarization or laminarization since the turbulent boundary layer becomes

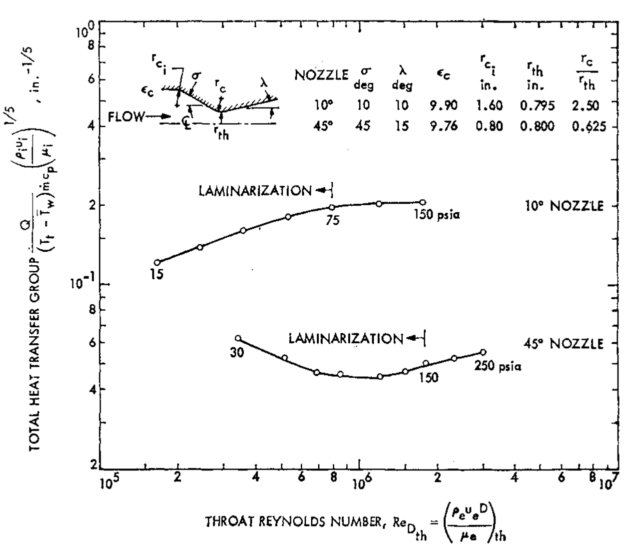

Fig. 10 Total heat-transfer group up to the throat for axial-inflow nozzles.

laminar-like near the wall. From a cooling point of view the reduced heat transfer accompanying this phenomenon is beneficial. With a nozzle that has a steeper convergent section (45°) there is also a reduction in heat transfer along the convergent section and in the throat region associated with laminarization.[8] This occurs at even higher throat Reynolds numbers for larger convergent half-angle nozzles.[16] However, the reduction in heat transfer along the latter part of the convergent section is offset by an increase in the total heat-transfer group as a consequence of flow separation and reattachment in the inlet region where the axial flow is compressed in turning to follow along the wall (adverse pressure gradient). The flow also separates in the inlet region of the 10° nozzle, but the length of the separation and reattachment region is relatively short compared to the length of the convergent section, and hence, is not of much consequence with regard to the total heat transfer.

Therefore, it would appear advantageous to design nozzles with fairly steep convergent sections to promote laminarization (they would also be shorter and weigh less) in those applications where laminarization might be expected to occur, but at the same time to try to avoid separation in the inlet region. This can be accomplished by allowing the flow to approach the nozzle radially inward instead of axially. Such a nozzle may also have a smaller combustion chamber surface area if used in a rocket and therefore the energy loss by heat transfer to the wall should be less.

Summary and Conclusions

Results obtained from wall static pressure measurements were presented for an axial inflow nozzle which had a relatively steep convergent section ($\sigma = 75°$) and a comparatively small radius of curvature at the throat ($r_c/r_{th} = 0.25$). There were large differences along the convergent and throat sections relative to a one-dimensional, isentropic, plane flow that was used as a reference datum; at the physical throat the Mach number near the wall was 1.7. Along the conical convergent section the higher pressures measured could be estimated by considering conical sink flow. Consequently, the thrust decrement for the entire nozzle as well as that for other axial inflow nozzles considered could be estimated fairly well, Eqs. (10) and (11), since the net contribution to the thrust decrement from the throat and divergent sections was essentially negligible.

The results obtained from wall static pressure measurements and pitot probe measurements in the radial inflow nozzle indicated that the flow accelerated in most of the radial inflow region located between the endwall and the plane portion of the nozzle wall where the flow cross-sectional area decreased as the flow progressed radially inward. Near the endwall it then decelerated and separated before reaching the center; however, it continued to accelerate near the nozzle wall and large deviations from one-dimensional, isentropic, plane flow were observed in the throat region primarily because of the throat configuration ($r_c/r_{th} = 0.49$).

The specific impulse relative to that for one-dimensional isentropic, plane flow was found to differ little from unity for the axial and radial inflow nozzles considered. However, because of the lower mass flow coefficients and thrust ratios it would be necessary to provide a higher chamber pressure or a larger throat diameter to obtain a given thrust, or a longer burn to achieve a given total impulse than for a conventional rocket nozzle.

In particular, the radial inflow nozzle appears to be attractive if used in a rocket engine, although heat-transfer measurements are required to appraise its potential advantage inferred from available heat-transfer measurements in nozzles with axial inflow.

References

[1] Back, L. H., Massier, P. F., and Gier, H. L., "Comparison of Measured and Predicted Flows Through Conical Supersonic Nozzles, with Emphasis on the Transonic Region," *AIAA Journal* Vol. 3, No. 9, Sept. 1965, pp. 1606–1614.

[2] Shelton, S. V., private communication, 1971.

[3] Norton, D., and Shelton, S., "Performance of Rocket Nozzles with Low Radius of Curvature Ratios," *Jet Propulsion Laboratory Space Programs Summary* 37–55, Vol. III, Pasadena, Calif., Feb. 1969, pp. 167–169.

[4] Strand, L., Newton, J. F., Jr., and Herrera, J. G., "Initial Performance of a New Nozzle Gas-Dynamics Test Facility," TM33-310, Nov. 1966, Jet Propulsion Lab., Pasadena, Calif.

[5] Cuffel, R. F., Back, L. H., and Massier, P. F., "Transonic Flow Field in a Supersonic Nozzle with Small Throat Radius of Curvature," *AIAA Journal*, Vol. 7, No. 7, July 1969, pp. 1364–1366.

[6] Back, L. H. and Cuffel, R. F., "Detection of Oblique Shocks in a Conical Nozzle with a Circular-Arc Throat," *AIAA Journal*, Vol. 4, No. 12, Dec. 1966, pp. 2219–2221.

[7] Back, L. H., Massier, P. F., and Cuffel, R. F., "Flow and Heat Transfer Measurements in Subsonic Air Flow Through a Contraction Section," *International Journal of Heat and Mass Transfer*, Vol. 12, No. 1, Jan. 1969, pp. 1–13.

[8] Back, L. H., Massier, P. F., and Cuffel, R. F., "Flow Phenomena and Convective Heat Transfer in a Conical Supersonic Nozzle," *Journal of Spacecraft and Rockets*, Vol. 4, No. 8, Aug. 1967, pp. 1040–1047.

[9] Prozan, R. J., "Transonic Flow in a Converging-Diverging Nozzle," LMSC/HREC D162177, Contract NAS7-743, 1970, Lockheed Missiles and Space Co., Huntsville, Ala.

[10] Prozan, R. J., and Kooker, D. E., "The Error Minimization Technique with Application to Transonic Nozzle Solution," *Journal Fluid Mechanics*. Vol. 43, Pt. 2, Aug. 1970, pp. 269–277.

[11] Back, L. H., and Cuffel, R. F., "Flow Coefficients for Supersonic Nozzles with Comparatively Small Radius of Curvature Throats," *Journal of Spacecraft and Rockets*, Vol. 8, No. 2, Feb. 1971, pp. 196–198.

[12] Wright, D. H., "Investigation of the Effects of Various Nozzle Transition Arc Radius Ratios," (Contract NAS7-706), March 1969, Thiokol Chemical Corp., Wasatch Div., Brigham City, Utah.

[13] Durham, F. P., "The Performance Characteristics of Small Rocket-Type Nozzles," Reps. 2, 3, and 6, 1953-1955, AD-58467, AD-58468 Contract N-123S-82337, T.O. 1, Univ. of Colorado, Boulder, Colo.

[14] Durham, F. P., "Thrust Characteristics of Underexpanded Nozzles," *Jet Propulsion*, Vol. 25, No. 12, Dec. 1955, pp. 696–700.

[15] Back, L. H., Cuffel, R. F., and Massier, P. F., "Laminarization of a Turbulent Boundary Layer in Nozzle Flow—Boundary Layer and Heat Transfer Measurements with Wall Cooling," *Transactions of the ASME, Ser. C, Journal Heat Transfer*, Vol. 92, No. 3, Aug. 1970, pp. 333–344.

[16] Back, L. H., Massier, P. F., and Cuffel, R. F., "Some Observations on Reduction of Turbulent Boundary-Layer Heat Transfer in Nozzles," *AIAA Journal*, Vol. 4, 1966, pp. 2226–2229.